Received: 18 April 2024 | Accepted: 10 July 2024

DOI: 10.1111/1462-2920.16680

BRIEF REPORT

ENVIRONMENTAL MICROBIOLOGY

A mesophilic relative of common glacier algae, *Ancylonema palustre* sp. nov., provides insights into the induction of vacuolar pigments in zygnematophytes

Anna Busch[1] | **Emilia Slominski**[1] | **Daniel Remias**[2] | **Lenka Procházková**[3] | **Sebastian Hess**[1,4]

[1]Department of Biology, University of Cologne, Cologne, Germany

[2]Department of Environment & Biodiversity, University of Salzburg, Salzburg, Austria

[3]Department of Ecology, Faculty of Science, Charles University, Prague, Czech Republic

[4]Department of Biology, Technical University of Darmstadt, Darmstadt, Germany

Correspondence
Anna Busch, Department of Biology, University of Cologne, Zülpicher Str. 47b, 50674 Cologne, Germany.
Email: anna.busch@uni-koeln.de

Funding information
Deutsche Forschungsgemeinschaft, Grant/Award Numbers: 417585753, 491244984; University Research Centers (UNCE) at the Charles University, Grant/Award Number: UNCE/24/SCI/006; Czech Science Foundation, Grant/Award Number: 24-10019S; Austrian Science Fund, Grant/Award Number: P34073

Abstract

The green algae of the genus *Ancylonema*, which belong to the zygnematophytes, are prevalent colonizers of glaciers worldwide. They display a striking reddish-brown pigmentation in their natural environment, due to vacuolar compounds related to gallic acid. This pigmentation causes glacier darkening when these algae bloom, leading to increased melting rates. The *Ancylonema* species known so far are true psychrophiles, which hinders experimental work and limits our understanding of these algae. For instance, the biosynthesis, triggering factors, and biological function of *Ancylonema*'s secondary pigments remain unknown. In this study, we introduce a mesophilic *Ancylonema* species, *A. palustre* sp. nov., from temperate moorlands. This species forms the sister lineage to all known psychrophilic strains. Despite its morphological similarity to the latter, it exhibits unique autecological and photophysiological characteristics. It allows us to describe vegetative and sexual cellular processes in great detail. We also conducted experimental tests for abiotic factors that induce the secondary pigments of zygnematophytes. We found that low nutrient conditions combined with ultraviolet B radiation result in vacuolar pigmentation, suggesting a sunscreen function. Our thriving, bacteria-free cultures of *Ancylonema palustre* will enable comparative genomic studies of mesophilic and extremophilic zygnematophytes. These studies may provide insights into how *Ancylonema* species colonized the world's glaciers.

INTRODUCTION

The conjugating green algae (Zygnematophyceae) comprise about 4000 described species with rather simple growth forms, ranging from non-flagellated unicells to filaments (Brook & Williamson, 2010; Coesel & Meesters, 2007; Hall & McCourt, 2015). As revealed by several phylogenomic studies, these algae are the closest relatives of land plants and hence important research subjects for understanding the transition from aquatic to terrestrial life (Timme et al., 2012; Wickett et al., 2014; Wodniok et al., 2011). Of particular interest are physiological adaptations to terrestrial conditions that potentially predated the origin of the land plants and thereby facilitated their evolution (de Vries et al., 2017, 2020; Fürst-Jansen et al., 2020). Most zygnematophytes thrive in freshwater-fed systems of various trophic levels, including ponds, lakes and moorlands. However, some lineages colonize more extreme habitats such as rock surfaces, deadwood, tree bark, and even glacial ice (Busch & Hess, 2022a; Remias et al., 2009). Only very few known zygnematophytes adapted to the freezing temperatures and high solar radiation that exist on glaciers. The two most

widespread zygnematophyte species inhabiting such extreme habitats are *Ancylonema nordenskioeldii* and *A. alaskanum* (Procházková et al., 2021). They have been found on glaciers of the European Alps, Greenland, Alaska, Svalbard, the Altai Mountains, the Himalaya and Antarctica (Kol, 1942; Ling & Seppelt, 1990; Remias et al., 2009; Takeuchi, 2001; Takeuchi et al., 2006, 2019; Williamson et al., 2018; Yoshimura et al., 1997), and occasionally grow at high densities. In recent years, glacier algae gained much attention, since their blooms have detrimental effects on glaciers. A dark cover of algal cells, anthropogenic black carbon and mineral debris reduces the albedo of glacial ice surfaces, absorbs solar radiation and thereby accelerates glacial melting during summer (Cook et al., 2020; Stibal et al., 2017; Williamson et al., 2018, 2019; Yallop et al., 2012). The colouration caused by *Ancylonema* blooms results, in part, from reddish-brown, non-photosynthetic pigments, which accumulate in vacuoles of the algal cells (Remias et al., 2009). These secondary pigments are of phenolic origin, and a main compound from *A. alaskanum* was previously identified as purpurogallin carboxylic acid-6-O-β-D-glucopyranoside, which shows a broad absorbance in the UV–VIS portion of sunlight (Remias, Schwaiger, et al., 2012). In the natural habitat, these phenolics equip the algal cells with a remarkable, dark brown colouration. Hence, several biological functions of *Ancylonema*'s secondary pigments have been proposed, including a function as sunscreen, chemical defence agent, and ice-melting agent (Dial et al., 2018; Remias, Schwaiger, et al., 2012). A photoprotective function seems most likely, as these compounds very effectively absorb UVR and VIS and are supposed to shade the low-light-adapted chloroplasts (Williamson et al., 2020). However, this hypothesis was never experimentally tested as the psychrophilic nature of the known *Ancylonema* species is a hurdle for experimental research. The recently established cultures depend on low temperatures (≤5°C), grow very slowly and are not axenic (Jensen et al., 2023; Remias & Procházková, 2023). So far, we lack any knowledge about the biosynthetic pathway of intracellular pigments of zygnematophytes and the environmental factors that trigger their biosynthesis.

In the temperate moorlands of Germany, we discovered mesophilic *Ancylonema* strains, which showed a remarkable resemblance to their psychrophilic relatives, including the reddish-brown intracellular pigmentation. We established well-growing, axenic cultures, which were used to pinpoint the evolutionary origin of these algae by molecular phylogenetics and to characterize the vegetative cell cycle and sexual processes, including zygospore formation. Furthermore, we studied the photosynthetic performance of the mesophilic strains and tested abiotic factors (nutrient conditions, light regimes) for their effect on the biosynthesis of secondary pigments. Overall, this is the first report and detailed characterization of a mesophilic *Ancylonema* species, here described as *A. palustre* sp. nov., setting the ground for future comparative genomic and ecophysiological studies.

EXPERIMENTAL PROCEDURES

Collection and cultivation of algae

Natural samples were collected at two moorlands in Germany (see Table S1 for detailed sampling information) and screened for algal cells. Single cells were isolated with a micropipette under visual control with a Motic AE2000 inverted microscope (Motic, Hong Kong), washed in sterile water, and transferred into the liquid growth medium Waris-H (McFadden & Melkonian, 1986). The isolated cells were incubated at low, artificial light from white LEDs (<30 μmol photons m^{-2} s^{-1}), which resulted in well-grown cultures. These cultures were used to establish bacteria-free strains by spray-plating as previously described (Busch & Hess, 2022a). The bacteria-free cultures were grown at 15°C under a 14/10 h light/dark cycle with a photon fluence rate of about 30 μmol photons m^{-2} s^{-1} photosynthetically active radiation (PAR) supplied by LinearZ SunLike LEDs (5700 K, Lumitronix, Hechingen; see Figure 1A for spectral power distribution). The established algal strains, N3 and V5, are available through the Central Collection of Algal Cultures (CCAC) based at the University of Duisburg-Essen under the accession numbers CCAC 9547 (N3) and CCAC 9548 (V5).

Light and scanning electron microscopy

Time-lapse microscopy and photodocumentation of experimental cultures were done with the Motic AE2000 inverted microscope (Motic, Hong Kong) equipped with a MikroLive 6.4MP CMOS camera (MikroLive, Oppenau). For high-resolution imaging, the Zeiss Axio Observer inverted microscope equipped with the objective lenses Plan-Neofluar 40×/1.3 and Plan-Neofluar 100×/1.3 and the Axiocam 512 colour (Carl Zeiss, Oberkochen) was used. For scanning electron microscopy, cells were collected by sedimentation, fixed with 2.5% glutaraldehyde and 1% osmium tetroxide in MT buffer (30 mM HEPES, 15 mM KCl, 5 mM EGTA, 5 mM $MgSO_4$, pH 7), dehydrated in a graded series of ethanol:water mixtures, transferred into hexamethyldisilazane, and finally dried in the fume hood as previously described (Moye et al., 2022). The dry samples were sputter-coated with gold and examined with a ZEISS Neon 40 scanning electron microscope at 2.5 kV acceleration voltage (Carl Zeiss, Oberkochen).

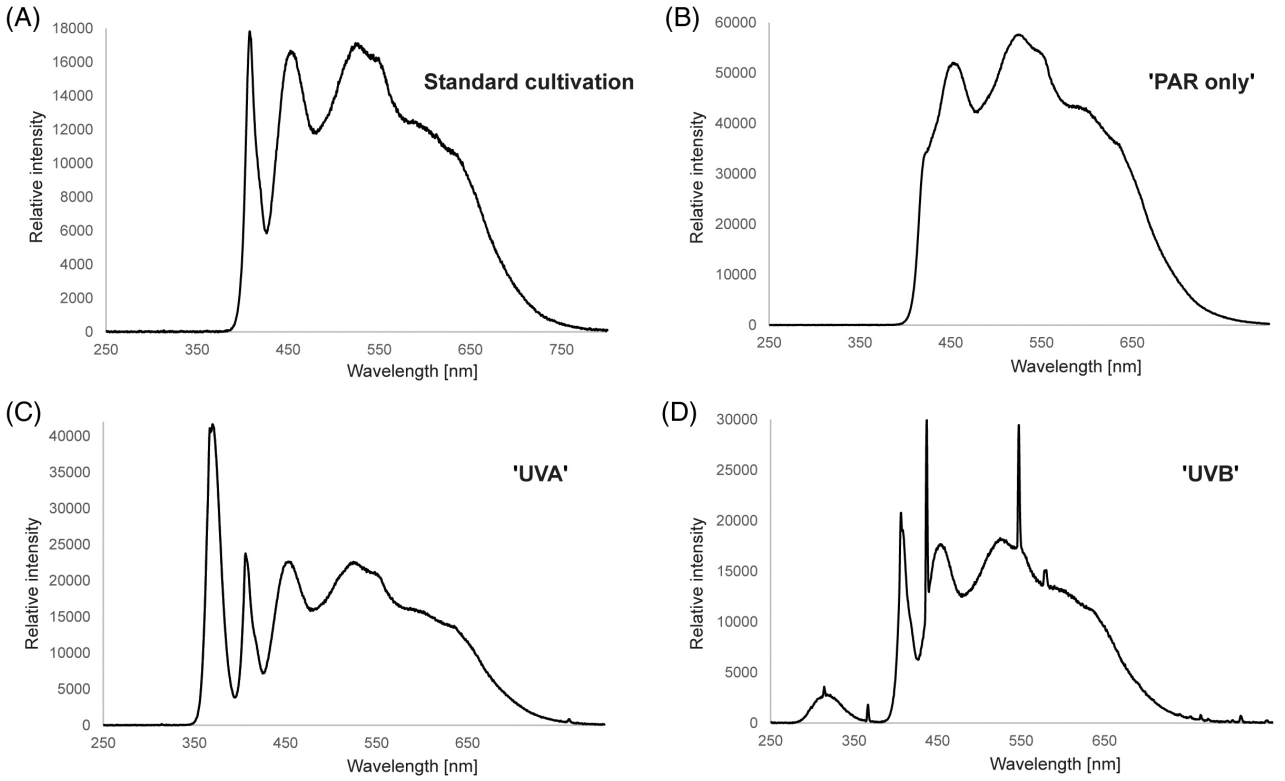

FIGURE 1 Spectral emittance of the applied light sources measured through the lids of the culture containers in which the experiments were conducted. (A) Standard cultivation (LinearZ SunLike LEDs, 5700 K). (B) 'PAR only' treatment (SunLike high-power LED 5000 K, 50 W). (C) 'UVA' treatment (TL-D Blacklight Blue fluorescent tube lamp, 18 W + LinearZ SunLike LEDs, 5700 K). (D) 'UVB' treatment (UVB Broad Band TL, 20 W + LinearZ SunLike LEDs, 5700 K).

The brightness and contrast of micrographs were adjusted with Photoshop CS4 (Adobe Inc., Dublin).

DNA sequencing, alignment and molecular phylogenetics

Algal material from 15 mL of an axenic culture was collected by centrifugation (500 *g*, 10 min), washed twice with sterile, ultrapure water, and again collected by centrifugation. The resulting pellet was snap-frozen in liquid nitrogen and lyophilized with the freeze-drying system BETA 1–8 LD plus (Christ, Osterode am Harz). Twenty SiLibeads Type ZY 6.0 of about 3 mm (Sigmund Lindner GmbH, Warmensteinach) were added to each sample, followed by mechanical lysis of the freeze-dried cells in a TissueLyser II (QIAGEN, Hilden). The samples were subjected to 2 min of shaking with a frequency of 30 min^{-1}. To extract DNA, the samples were further processed with the DNeasy PowerLyzer PowerSoil Kit (QIAGEN, Hilden) according to the manufacturer's instructions. The chloroplast encoded gene for the RuBisCO large subunit (*rbc*L) was amplified by a semi-nested PCR with the primers MaGo1F, MaGo2F and MaGo3R as previously described (Busch & Hess, 2022a; Gontcharov et al., 2004). The nucleus-encoded gene for the 18S rRNA was amplified with the universal eukaryotic primers EukA and EukB (without terminal polylinker; [Medlin et al., 1988]) after the following protocol: initial denaturation (95°C, 180 s), followed by 35 cycles of denaturation (95°C, 45 s), annealing (55°C, 60 s), and elongation (72°C, 180 s). All PCRs were done with the Taq DNA Polymerase (Invitrogen, Waltham, MA) according to the manufacturer's protocol. The PCR products were subjected to commercial Sanger sequencing (Eurofins Genomics, Ebersberg) with the primers MaGo2F and MaGo3R (*rbc*L gene) and EukA and EukB (18S rRNA gene). The nearly complete *rbc*L and 18S rRNA gene sequences were assembled and subsequently aligned with available gene sequences of other Zygnematophyceae as previously described (Busch & Hess, 2022a). Sequences are deposited at GenBank (https://www.ncbi.nlm.nih.gov/genbank/) under the accessions PP555606, PP555607, PP555608 (*rbc*L gene) and PP544794, PP544795 (18S rRNA gene). For the *rbc*L gene, we used an existent alignment (Busch & Hess, 2022a), while 18S rRNA gene sequences were retrieved from the National Center for Biotechnology Information (https://www.ncbi.nlm.nih.gov/). This resulted in two final datasets: (1) 35 zygnematophycean *rbc*L gene sequences with 1290 sites, and

(2) 15 zygnematophycean 18S rRNA gene sequences with 1675 sites. They were subjected to phylogenetic inferences with maximum likelihood (ML), neighbour joining (NJ) and maximum parsimony (MP) methods using the MEGA11 software (Tamura et al., 2021). The ML analyses were done with the GTR + I + G model (discrete Gamma distribution; five categories), NJ analyses with the P-distance model with the 'partial deletion' option, and MP analyses with the Subtree-pruning-regrafting (SPR) algorithm. To assess the statistical support of the branches, we performed 1000 bootstrap repetitions for every analysis and added the resulting values to the ML topology shown in the results and the supplements. A pairwise distance analysis of six selected *rbc*L gene sequences was performed with 1304 sites. All codon positions were included, but ambiguous positions were removed for each sequence pair (pairwise deletion option).

Pulse–amplitude modulated fluorometry

Cells of strains N3 and V5 were grown in Waris-H medium under the standard culturing conditions (see above) and then acclimated to two light conditions (12/12 h light/dark cycle), here termed 'low light' (PAR: 19–22 μmol photons m^{-2} s^{-1}, UVA: 0.05–0.06 W m^{-2}, UVB: 0.005–0.006 W m^{-2}) and 'high light' (PAR: 140–170 μmol photons m^{-2} s^{-1}, UVA: 0.3 W m^{-2}, UVB 0.02–0.03 W m^{-2}) for 1 week. During acclimatization, the cells were kept at 15°C and agitated by shaking at 150 rpm. After harvesting by sedimentation, the cells were subjected to pulse–amplitude modulated fluorometry with a Walz PAM 2500 in a KS-2500 suspension cuvette (0.4 mL) at 15°C. To determine the relative electron transport rates (rETR) of photosystem II, the apparent quantum yield for electron transport (α) and the light saturation point (I_k), we performed rapid light curve (RLC) measurements with photon flux densities (PFD) of 5, 34, 67, 104, 201, 366, 622, 984, 1389, 1666 and 2018 μmol photons m^{-2} s^{-1} for 30 s each. For each density, four independent replicates were measured. Data analysis was done as previously described (Procházková et al., 2018).

High PAR treatments

Algal material (strain N3) in the exponential growth phase was suspended in liquid KW medium (recipe in Table S2) and thereby diluted so that the cells could not shade each other. Suspended algal cells were evenly distributed in 35 mm tissue culture dishes (Sarstedt, Nümbrecht). The light experiments were started the following day and the cells were exposed to the SunLike high-power LED (5000 K, 50 W, Seoul Semiconductor, Ansan) in a 14/10 h light/dark cycle (see Figure 1B for spectral power distribution). Spectral power distributions were measured with the LR2 spectrometer (range 200–1200 nm) equipped with a patch cable, 365 μm fibre diameter (both Lasertack, Fuldabrueck). Measurements were done through the lids of the culture containers in which the experiments were conducted. Different irradiance settings (100–1300 μmol photons m^{-2} s^{-1}) were realized by adjusting the distance to the lamp. The algal cells were observed and photo-documented over at least 14 days. PAR irradiance was measured with the MQ-500 Full-Spectrum Quantum Sensor (Apogee Instruments Inc., Utah) through the lids of the used Petri dishes. The experiments were done in triplicates.

UVR treatments

Algal material (strain N3) in the exponential growth phase was suspended in liquid KW medium (see Table S2 for recipe) and thereby diluted, so that the cells could not shade each other. Suspended algal cells were evenly distributed to 100 mm tissue culture dishes (VWR International, Darmstadt). The light experiments were started the following day. The 'UVA treatment' was achieved with the TL-D Blacklight Blue fluorescent tube lamp (18 W, Philips, Hamburg), and the 'UVB treatment' with the UVB Broad Band TL (20 W, Phillips, Hamburg). For both treatments, cells were exposed for 4 h during the light phase of a 14/10 h light/dark cycle with PAR emitted by LinearZ SunLike LEDs (5700 K, Lumitronix, Hechingen) (see Figure 1C,D for spectral power distribution). Because of the absorbance of the Petri dish lids, the algae were not exposed to UVC radiation (transmission spectra of polystyrene Petri dish lids were previously recorded; Busch & Hess, 2022b). Different irradiance settings (1–8 W m^{-2} for UVA, 0.2–2.0 W m^{-2} for UVB) were realized by adjusting the distance to the lamps. The algal cells were observed and photo-documented over at least 14 days. UVA and UVB irradiances were measured with the digital UV radiometers Solarmeter® Model 4.2 and Solarmeter® Model 6.2, respectively (Solar Light Company Inc., Pennsylvania) through the lids of the Petri dishes. The experiments were done in triplicates.

Nutrient limitation treatments

We designed three variations of the KW medium, which were limited in nitrate (−N), phosphate (−P) or both (−P−N) (see Table S2 for recipes). Algal material (strain N3) in the exponential growth phase was concentrated by sedimentation and suspended in these liquid media, distributed in six-well tissue culture plates (VWR International, Darmstadt), and subjected to different light regimes. The latter included treatment with

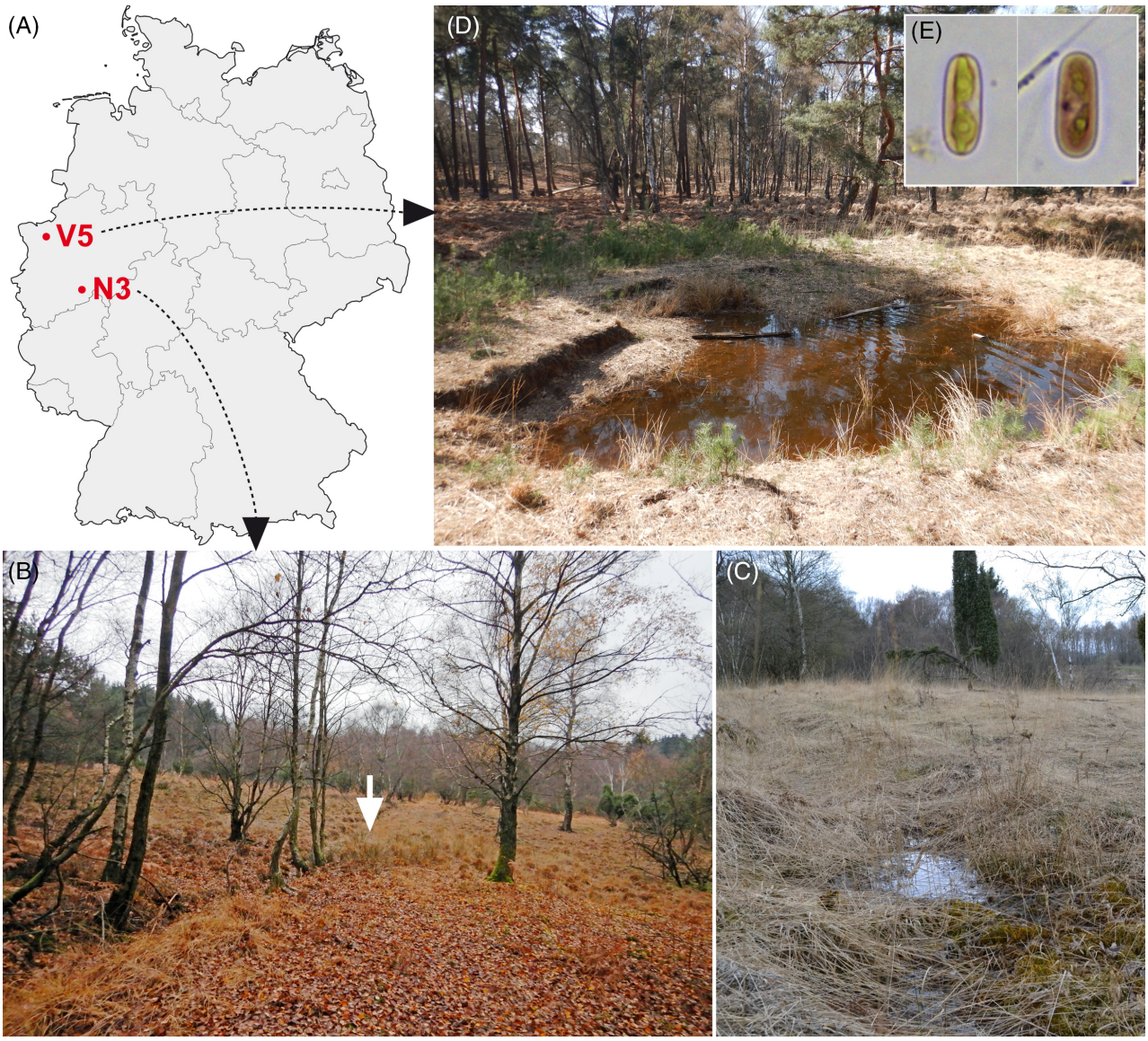

FIGURE 2 Collection sites of the studied *Ancylonema palustre* strains. (A) Map of Germany showing the two moorlands from which the algal strains (N3 and V5) were isolated. (B, C) Spring bog of Neuenhähnen, Germany. The white arrow denotes a waterlogged area with *Sphagnum* (shown in (C)), from which strain N3 was isolated. (D) Shallow bog pond with brownish water of the Großes Veen, Hamminkeln, Germany. Strain V5 was isolated from the oxygenated sediment. (E) The natural material of *A. palustre* from the pond shown in (D) with pronounced secondary pigmentation.

moderate/high PAR (200 µmol photons m^{-2} s^{-1}), UVA at 8 W m^{-2}, and UVB at 0.6 W m^{-2} (selected based on our previous experiments with varying irradiances). The experiments were done in triplicates and cells were photo-documented over at least 14 days.

RESULTS

Habitat characteristics and natural material

Two monoclonal and axenic strains of *Ancylonema palustre* (N3 and V5) were established in this study. Both strains derive from moorlands in western Germany (Figure 2A). The strain N3 was isolated from squeezed *Sphagnum* moss of a waterlogged area in the spring bog of Neuenhähnen, Waldbröl, Germany (Figure 2B,C). The strain V5 was found in the organic, oxygenated sediment of a shallow bog pond with acidic, brown water, close to a disturbed raised bog system of the moorland Großes Veen, Hamminkeln, Germany (Figure 2D). Cells from this site displayed reddish-brown cytoplasm (Figure 2E), which was lost during cultivation. The climate of both sampling sites is temperate/oceanic (annual temperature average: Neuenhähnen 9.4°C, Hamminkeln 10.8°C) with considerable rainfall (>850 mm $year^{-1}$), classified as Cfb after Köppen (Geiger, 1954).

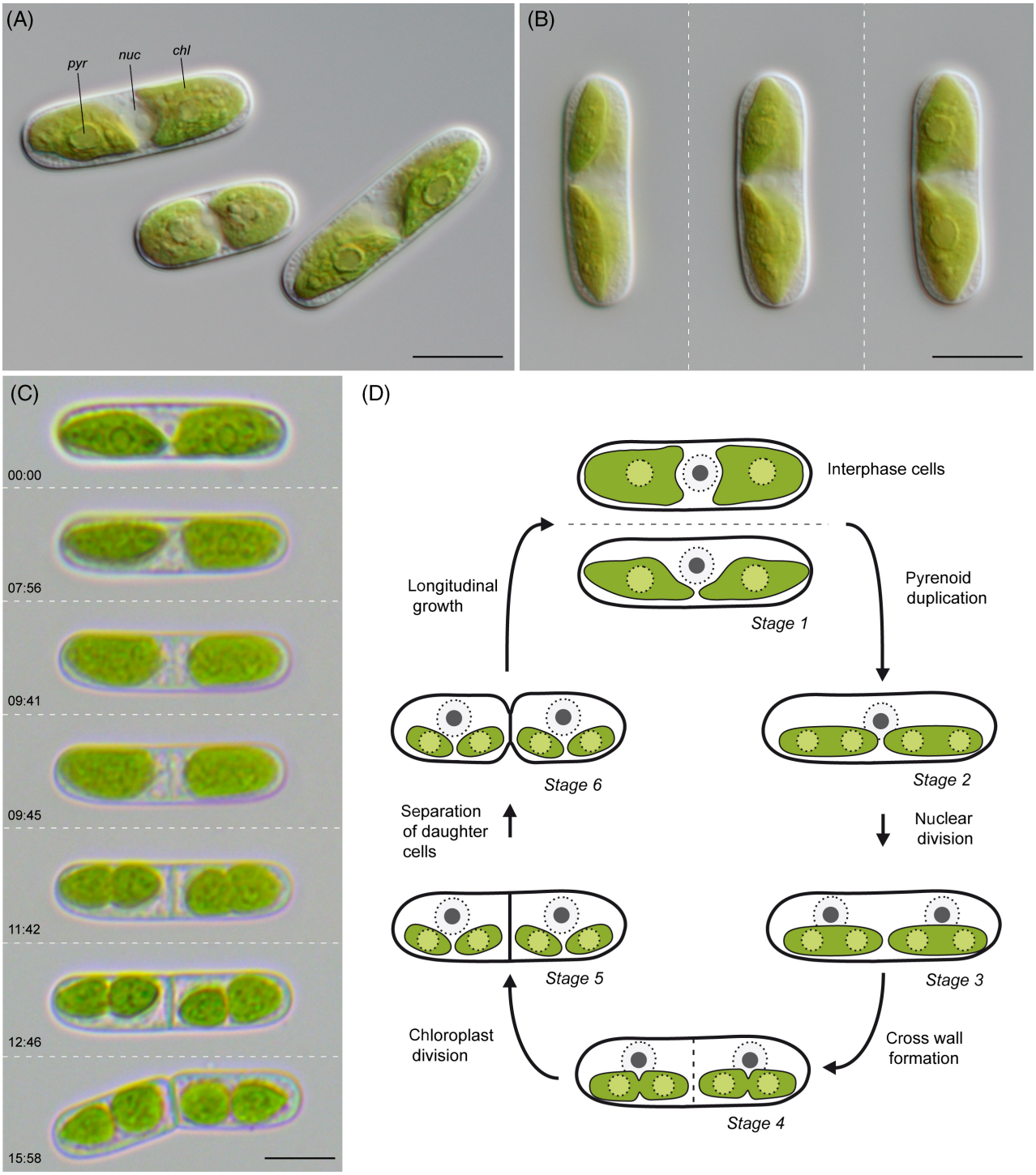

FIGURE 3 Morphology and cell division of *Ancylonema palustre*. (A) Cells of strain N3 under standard cultivation conditions. The nucleus (nuc) lies between two well-separated chloroplasts (chl), each of which contains a circular pyrenoid (pyr). (B) *A. palustre* cell (strain N3) shown in three focal planes. (C) Time series of cell division in strain N3 (time shown in mm:ss). (D) Generalized scheme of cell division in *A. palustre*. Scale bars: 10 μm.

Morphology and cell division

Vegetative cells from laboratory cultures were bright green and rod-shaped with rounded cell poles (Figure 3A). Cells of both strains were very similar in size, with a cell width of around 7 μm and a cell length ranging from 16 to 34 μm ($n = 100$, see Figure S1 for boxplots). While the cell width appeared to be relatively uniform, the cell length varied considerably due to cell growth between cell divisions. At interphase, each cell

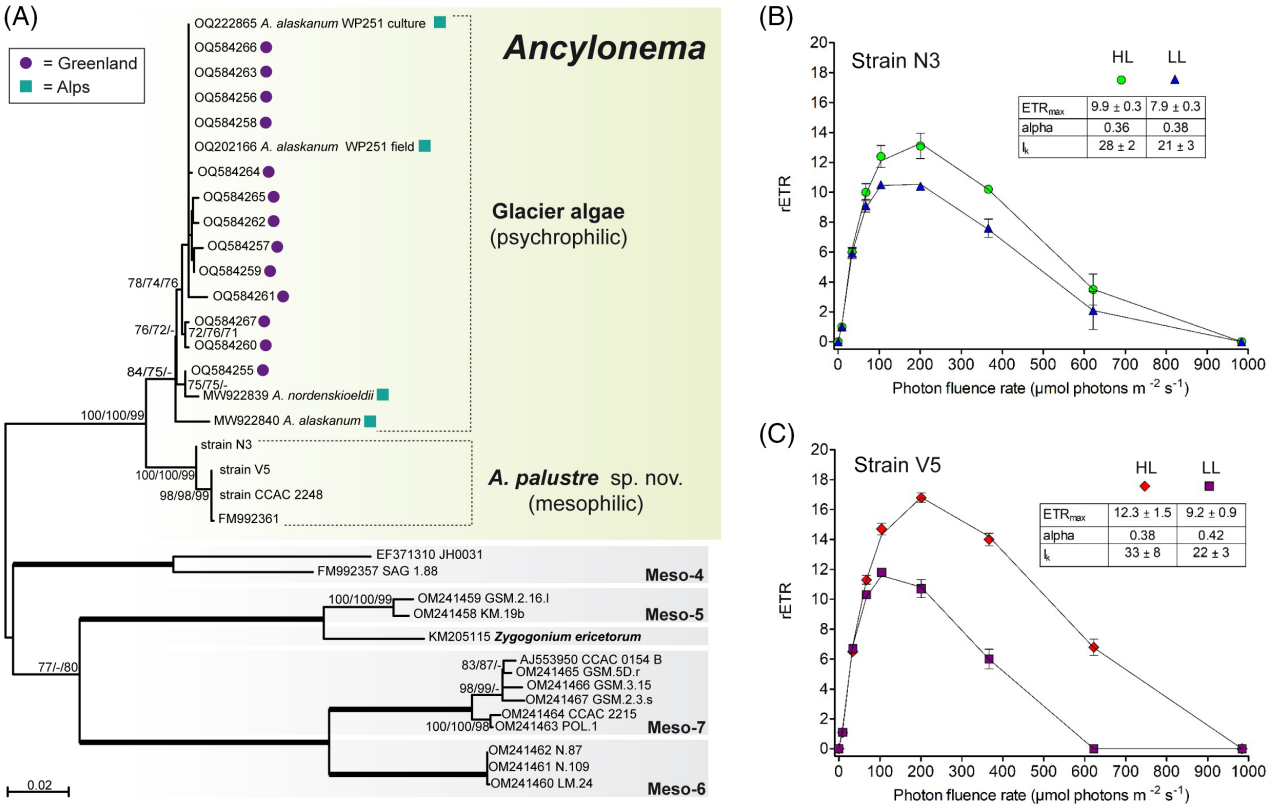

FIGURE 4 Phylogenetic position and photophysiology of *A. palustre*. (A) Maximum likelihood phylogeny of 35 zygnematophycean *rbc*L gene sequences displaying the relationships within the genus *Ancylonema*. Sequences from psychrophilic *Ancylonema* strains stem either from the Greenland ice sheet (violet circles) or the European Alps (blue squares). Support values >70% from different analyses (ML/NJ/MP) are shown on the respective branches. Branches with maximum support (100/100/100) are bold. The scale bar represents 0.02 nucleotide substitutions per site. (B, C) Rapid light curves of *A. palustre* strains N3 (B) and V5 (C), and deduced parameters (rETR = relative electron transport rate, α = low light utilization efficiency, and I_k = light compensation point). Both strains were measured after acclimatization to 'high light' (HL; green circles and red diamonds) and 'low light' (LL; blue triangles and violet squares). Values are means of four replicate measurements and the datapoints were fitted to the photoinhibition model of Walsby (1997).

contained a single nucleus of about 3.6 µm in diameter ($n = 40$) with a spherical nucleolus of about 1.7 µm ($n = 40$). The nucleus was located in the cell's centre between two chloroplasts (Figure 3A,B). These chloroplasts were mostly parietal and shovel-shaped with smooth margins, and there was no sign of a connecting bridge between them (Figure 3B). Each of the chloroplasts typically contained a single, circular or slightly elliptic pyrenoid of about 2.5 µm in diameter ($n = 80$; Figure 3B). Only rarely, we observed additional smaller pyrenoids. Time-lapse microscopy revealed the sequence of cellular events during the cell cycle (Figure 3C, Movie S1: https://zenodo.org/doi/10.5281/zenodo.12708605). The cell division started with the duplication of the pyrenoids, which was followed by nuclear division (Figure 3D, stages 1–3). The two new nuclei then migrated into the cell's halves and subsequently a cross wall was formed in the centre of the cell, starting with an increased vesicle movement (Figure 3D, stages 4, 5). Once the cross wall became more defined, the chloroplasts started to divide. The nearly synchronous divisions of the cell and the chloroplasts resulted in two firmly attached daughter cells with two chloroplasts each (Figure 3D, stage 5). The daughter cells separated slowly and attained the typical rod-shaped morphology by subsequent longitudinal cell growth (Figure 3D, stages 6, 1). We did not observe any pronounced formation of cell chains.

Molecular phylogeny

Figure 4A displays the best *rbc*L gene phylogeny (ML topology) of the genus *Ancylonema* plus selected outgroup lineages (Meso-4–Meso-7 and *Zygogonium ericetorum*). Our new strains N3 and V5 are closely related to an available *rbc*L sequence (FM992361) of an alga isolated from wet rock in a forest of the Eifel, Germany (A. Gontscharov, personal communication, no strain information available, Procházková et al., 2021). This alga might be identical to an uncharacterized algal strain of the Central Collection of Algal Cultures (CCAC2248), which was also sequenced in this study. Together, the four sequences

of mesophilic algae form a highly supported clade (100/100/99), whose members are here assigned to the new species *A. palustre*. The *A. palustre* clade shows a sister relationship to the known sequences from psychrophilic *Ancylonema* strains. This grouping is very robust as well (100/100/99), so we include the new, mesophilic strains in the genus *Ancylonema*. The subclade of psychrophilic representatives contains sequences from recently established cultures (OQ222865, OQ584255–OQ584267) as well as from field material (OQ202166, MW922839, MW922839). They stem from the Greenland ice sheet (violet circles) and the Alps (blue squares) and do not group according to their geographic origin. The *rbc*L gene phylogeny further reveals that the sequence MW922840, previously assigned to the species *A. alaskanum* (Procházková et al., 2021) is not identical or directly related to the cultivated *A. alaskanum* strain WP251 (Remias & Procházková, 2023). This points to some prevailing taxonomic problems concerning the species concepts of *A. alaskanum* and *A. nordenskioeldii*.

The mesophilic strains N3 and V5 showed only minor genetic differences in the *rbc*L gene. Pairwise distance analysis revealed a difference of <0.5% between the four *A. palustre* sequences, while the genetic difference between these sequences and those of *A. alaskanum* (OQ222865) and *A. nordenskioeldii* (MW922839) were 2.8% and 3%, respectively (Table S3 for details). Overall, we recognize two genetically distinct subclades of the genus *Ancylonema*, which correlate with the ecological preferences of the strains (psychrophilic vs. mesophilic). We also generated sequence data of the 18S rRNA gene and inferred an 18S rRNA gene phylogeny. Even though the taxon sampling was not as broad and the phylogenetic signal of the 18S rRNA gene relatively weak, we observed a split of psychrophilic and mesophilic *Ancylonema* species in two subclades as well (Figure S2).

Photophysiology of laboratory cultures

For both strains (N3, V5), we collected rapid light curves of cells acclimated to 'low light' and 'high light' conditions, respectively (Figure 4B,C). The maximum electron transport rate (ETR_{max}) was markedly higher in the high light-adapted cells, which also showed a slightly higher light saturation point (I_k). The low-light utilization efficiency α ranged from 36 to 42 in both strains, with higher values in low-light adapted cells. Both strains showed signs of photoinhibition irrespective of the acclimatization conditions. In strain N3 the onset of photoinhibition was at about 200 μmol photons m^{-2} s^{-1}, in strain V5 it was somewhat earlier at about 100 μmol photons m^{-2} s^{-1}. Overall, short-term acclimatization of *A. palustre* cells to higher light conditions resulted in lower α, higher I_k and enhanced ETR_{max}.

Cellular reactions to different light and nutrient conditions

Under our standard laboratory conditions (30 μmol photons m^{-2} s^{-1}; 15°C, Waris-H medium) the cells of *A. palustre* lost their reddish-brown, intracellular pigmentation. However, in very old cultures we observed the sporadic occurrence of slightly reddish cells, pointing to an effect of the nutrient availability on the production of secondary pigments. Furthermore, it is already established that other saccoderm desmids (*Serritaenia* spp.) can be triggered to form other dark sunscreen pigments (extracellular) by experimental UVB exposure (Busch & Hess, 2022b). To test whether the production of vacuolar pigments in *A. palustre* can be experimentally induced, we subjected cells of strain N3 to different light and nutrient conditions.

The cells were exposed to three different spectral power distributions, termed 'High PAR', 'UVA' and 'UVB' (Figure 1B–D), at varying irradiances, and showed distinct cellular reactions (Figure 5A–I). All three spectral ranges triggered the formation of vacuolar pigments (referred to as 'pigmentation' in the following) after 2–7 days but with very different effectiveness. While high PAR (>200 μmol photons m^{-2} s^{-1}) and UVA (>1 W m^{-2}) resulted in very faintly pigmentated cells (Figure 5C,F), UVB at >0.2 W m^{-2} led to a marked vacuolar pigmentation (Figure 5H,I). The varying extent of the dark pigmentation was confirmed with high-resolution brightfield microscopy (Figure 6A–C). Furthermore, we observed a significant shrinkage of the chloroplasts under very high PAR and UVB conditions (Figure 5C,I). High PAR (>500 μmol^{-2} s^{-1}) had clearly adverse effects on the cells, including the deformation and bleaching of the chloroplasts, the formation of unusual pigment inclusions (vacuoles of reddish-brown colour), and cell death (Figures 5C and S3A,B). The formation of pigment inclusions was also observed under very high UVA exposure (>8 W m^{-2}, Figure S3C,D).

The limitation of nitrate (–N) and phosphate (–P) in the culture medium showed clear effects on the cells of *A. palustre* under standard light conditions. While the absence of phosphate in the medium alone did not have any visible effect on the cells (Figure 5J), nitrate limitation led to the formation of large colourless globules within the cytoplasm (Figure 5K). The strongest effect was observed under combined phosphate/nitrate limitation (–P–N), including the formation of colourless globules and reddish cytoplasm. These effects were already apparent after 4 days of treatment but increased further with time (Figure 5L,M). High-resolution microscopy also revealed a pronounced shrinkage of the chloroplast under P/N limitation (Figure 6D).

Finally, we tested the cumulative effects of P/N limitation and three light conditions that triggered the

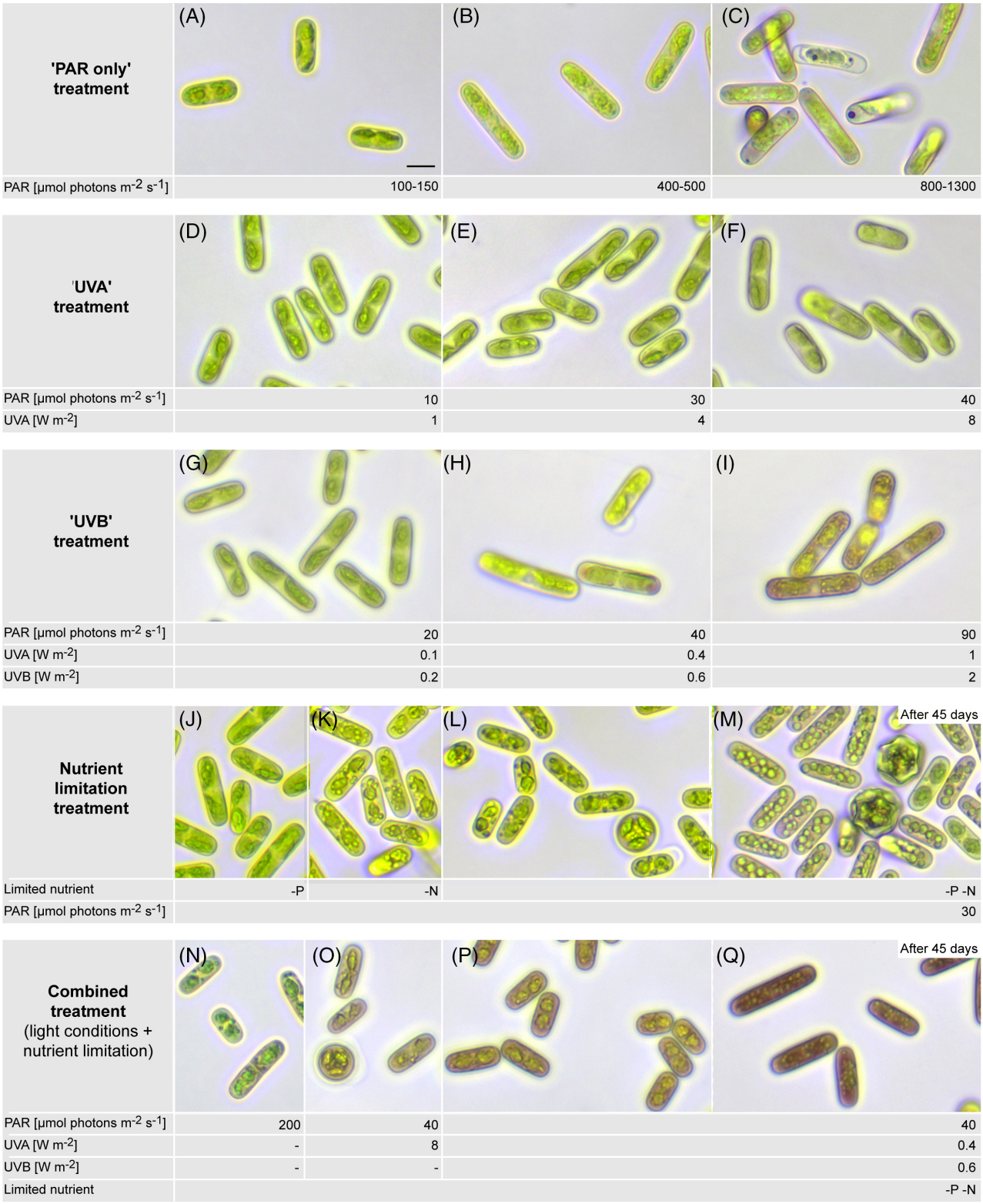

FIGURE 5 Phenotypic characteristics of *A. palustre* (strain N3) after 10 days of incubation (if not stated differently) under different light regimes and nutrient conditions. (A–C) Three selected irradiance levels of the 'PAR only' treatment. (D–F) Three selected irradiance levels of the 'UVA' treatment. (G–I) Three selected irradiance levels of the 'UVB' treatment. (J) KW medium without phosphate (–P). (K) KW medium without nitrate (–N). (L, M) KW medium without phosphate and nitrate (–P–N). (N–Q) P/N limitation combined with 'PAR only' (N), 'UVA' (O), and 'UVB' (P, Q) treatments. Scale bar: 10 µm.

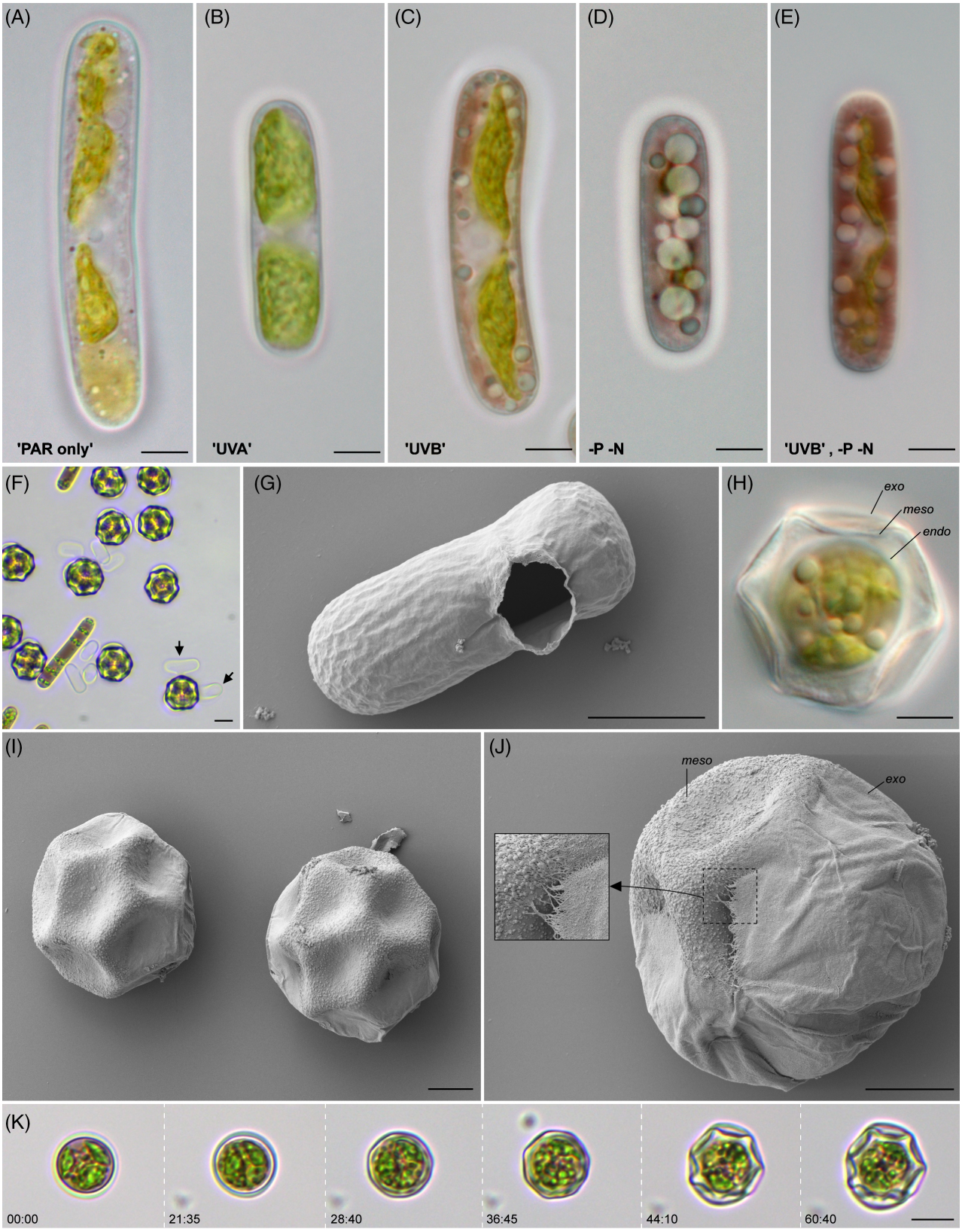

FIGURE 6 Legend on next page.

intracellular pigments but did not harm the cells (PAR: max. 200 μmol photons m^{-2} s^{-1}, UVA: max. 8 W m^{-2}, UVB: max. 0.6 W m^{-2}). All combinations led to pigmented cytoplasm (Figure 5N–P), which was most intense under the UVA and UVB treatments. After 45 days of treatment, cells under P/N limitation and UVB exposure displayed strongly coloured cytoplasm and relatively small but green chloroplasts, resembling the *Ancylonema* cells found in nature (Figures 5Q and 6E). Under all tested conditions the intracellular secondary pigments had a reddish colour.

Formation and morphology of zygospores

Under N limitation and P/N limitation both *A. palustre* strains formed roundish zygospores by conjugation of monoclonal cells, leaving behind two empty parental cell walls (Figure 6F). These cell walls exhibited a roundish hole with a dilatated margin of porous/fibrillar texture (Figure 6G). Mature zygospores measured 13–21 μm ($n = 20$) and had a multifaceted morphology with three discernible cell walls (Figure 6H). The latter may correspond to the exo-, meso- and endospore of other Zygnematophyceae (Permann et al., 2023). The inner zygospore wall (endospore) had a round outline and tightly surrounded the protoplast, while the middle wall (mesospore) created a polyhedral appearance by folds and/or ribs (Figure 6H). In scanning electron micrographs, it became apparent that the polygonal faces of the zygospores were not flat but rather represented depressions (Figure 6I). Most of the zygospores were likely to have 12 faces, as most observed faces had five adjacent faces (comparable to a dodecahedron). The surface of the polyhedral wall (mesospore) was granular due to fine warts, but in many cases partially covered by a smooth, skin-like envelope, the potential exospore (Figure 6J). This envelope appeared to be ruptured and displayed fairly long fibrils (potentially cellulose) at the edges (Figure 6J, inset). Time-lapse microscopy of the zygospore maturation revealed that the zygospores of *A. palustre* started as spherical cells with a smooth cell wall, which then increased in thickness and was subsequently slightly deformed by another secondary cell wall (Figure 6K, Movie S2: https://zenodo.org/doi/10.5281/zenodo.12708605). This secondary cell wall grew bigger and produced the polyhedral geometry of the zygospore. On top of this secondary wall were some remains of a smooth cell wall, which may correspond to the ruptured, skin-like layer observed in the scanning electron microscope. The formation of a third cell wall, which tightly surrounds the spherical protoplast could not be captured very well, but this is likely to be the last event during zygospore maturation (compare with Figure 6H).

DISCUSSION

Until now, *Ancylonema* species have only been known from glacial ice (rarely snow) and represent the best-studied psychrophilic streptophyte algae. Hence, the discovery of mesophilic *Ancylonema* strains from temperate moorlands raises the question of how they differ from the known species. From the morphological point of view, they appear similar at first glance. Both the psychrophilic species (*A. alaskanum* and *A. nordenskioeldii*) and the new mesophilic species form rod-shaped cells with rounded cell poles and contain shovel-shaped chloroplasts with smooth margins and circular pyrenoids. However, our morphological analysis revealed distinct differences concerning the cell width, the number of observed chloroplasts, conjugation and zygospore morphology. In the saccoderm desmids, the cell width appears to be a relatively stable character of taxonomic significance. This character can differ between genetically distinct strains but was shown to remain unaltered in natural versus cultivated material (Barcytė et al., 2020; Busch & Hess, 2022b). The new species *A. palustre* is more slender than the cultivated strain of *A. alaskanum* (7 μm vs. 8.5 μm) and the natural material of *A. nordenskioeldii* (>10 μm) (Procházková et al., 2021; Remias & Procházková, 2023). Our time-lapse studies on *A. palustre* revealed that this species (in culture) has always two chloroplasts per cell throughout the cell cycle. This is because the division of the chloroplasts coincides with the formation of a new cross wall. In natural and cultivated material of *A. alaskanum*, cells with only one chloroplast have frequently been documented (Procházková et al., 2021; Remias et al., 2009; Remias & Procházková, 2023). Of course, cell cycle processes might be influenced by environmental conditions and future in-depth studies on cultivated glacier species have to complete our picture. Under nutrient-poor conditions (esp. nitrate limitation), *A. palustre*

FIGURE 6 Phenotypes of *A. palustre* under different cultivation regimes and details of zygospore formation and structure. (A–E) Representative cells from cultures of strain N3 exposed to 'PAR only' (Figure 5C), 'UVA' (Figure 5F), 'UVB' (Figure 5I), P/N limitation (Figure 5M), and P/N limitation combined with 'UVB' (Figure 5Q). (F) Mixed culture of strains N3 and V5 with mature zygospores, which are sometimes attached to empty parent cell walls (black arrows). (G) Scanning electron micrograph of an empty cell (strain V5) with a nearly circular hole after release of the gamete. (H) Mature zygospore (strain V5) with three distinctive cell walls, namely exospore (exo), mesospore (meso) and endospore (endo). (I) Scanning electron micrograph of two mature zygospores (strain V5) revealing the dodecahedron-like morphology. (J) Scanning electron micrograph of a zygospore (strain N3) with ruptured exospore (exo). (K) Time series of zygospore maturation in strain V5 (time shown in mm:ss). Scale bars: 5 μm in (A–E), (G–J); 10 μm in (F and K).

forms zygospores by conjugation of monoclonal cells, which exit the parent cell walls during the process and form a spherical zygote. This effect of nitrate limitation is consistent with published observations on other genera, for example *Mesotaenium*, *Spirogyra* and *Closterium* (Hogetsu & Yokoyama, 1979; Tiflickjian & Raybum, 1986; Yamashita & Sasaki, 1979; Zwirn et al., 2013). The zygote of *A. palustre* develops into a zygospore with three cell wall layers, which correspond to the endo-, meso- and exospore layers (Permann et al., 2023). The relatively thick mesospore of *A. palustre* exhibits a remarkable, multifaceted morphology, most closely resembling a dodecahedron. In some other species (e.g., *Spirogyra* and *Mougeotia*) the mesospore was shown to contain lipids and aromatic compounds and is thought to be responsible for the high resistance of zygospores against environmental factors (Permann et al., 2022; Permann, Herburger, Felhofer, et al., 2021; Permann, Herburger, Niedermeier, et al., 2021). Furthermore, the mesospore represents a defining character of taxonomic value, as it can vary in colour (e.g. brown, yellow and purple), shape and ornamentation depending on the species (Pichrtová et al., 2018; Poulíčková et al., 2007; Takano et al., 2019). As far as we know, mature zygospores have not been documented for the psychrophilic *Ancylonema* species. However, Remias, Holzinger, et al. (2012) found conjugating *A. nordenskioeldii* cells, which apparently do not exit the parent cells and, thereby, produce more irregular zygotes with a prominent conjugation bridge. There is another account for zygospores of psychrophilic *Ancylonema* strains from continental Antarctica (Ling & Seppelt, 1990). These algae, referred to as '*Mesotaenium berggrenii*', lack any genetic information and show a conspicuous variation in cell sizes, potentially pointing to more than one species. In contrast to *A. nordenskioeldii*, the documented zygotes are spherical. As they have a smooth cell wall and no discernible mesospore, they might be immature and further studies have yet to show whether these psychrophilic strains form multifaceted mesospores similar to those of *A. palustre*.

The molecular phylogenies of two marker genes (*rbc*L, 18S rRNA) confirm the separation of mesophilic and psychrophilic *Ancylonema* species, which form two distinct clades and show clear genetic divergence in the *rbc*L gene (>2.8%). Hence, we are confident in proposing a new species for the three mesophilic *Ancylonema* strains (N3, V5, CCAC2248), accepting minor genetic differences (<0.5%) among them, as we did not recognize any marked phenotypic differences. The taxonomic situation in the psychrophilic clade appears to be more difficult. Both psychrophilic morphospecies *A. nordenskioeldii* and *A. alaskanum* are part of a genetically shallow branch of sequences from environmental samples and crude cultures, that still lack a sound taxonomic treatment (Jensen et al., 2023). Furthermore, two separate isolates assigned to *A. alaskanum* occupy distinct positions, being non-monophyletic (MW922840 and sequences of WP251). The sequences were derived from the same Austrian glacier but were sampled in different years (2017 and 2020). Overall, the genetic variation visible in the psychrophilic clade indicates that the actual diversity of these algae might be greater than reasonably represented by only two described species. The morphological variability of *Ancylonema* cells in the field, for example the range of cell width (4–12 μm) observed by different authors for cells assigned to *A. alaskanum* (Remias et al., 2009), supports this hypothesis, and just recently Remias et al. (2023) recognized another undescribed species in glacier ice samples from Svalbard, the Alps of Switzerland and Austria, and Sweden by environmental ITS2 sequencing (reference ITS2 sequence: PP138441). We conclude that the genus *Ancylonema* probably hides more species than currently recognized, which deserve to be characterized by integrative taxonomy and ecophysiological studies in the future.

The strains of the two main *Ancylonema* clades occur in very different habitats. While glacial habitats are characterized by low temperatures close to the freezing mark, moorlands (including ponds) in the sampled zones can warm up considerably during summer (the maximum ambient temperatures in these zones are well above 15°C). This climatic difference is reflected by the preferred temperatures of the available *Ancylonema* cultures. While *A. alaskanum* dies at temperatures above 10°C (D. Remias, unpublished observation), *A. palustre* grows well at 15°C and higher. Furthermore, the two habitat types differ strongly in the level of solar radiation experienced by the algae. The lower altitudes of the sampled moorlands, potential shading by plants, debris and sediment, and absorbance by the water column (especially when humic substances are present) should reduce light and UV irradiances considerably (as compared to glacier surface habitats).

Our photophysiological measurements show that the two mesophilic *Ancylonema* strains (N3 and V5) reacted similarly at higher irradiances if grown under 'low light' conditions: The onset of photoinhibition (a decline in rETR) was noticed. This happened at relatively low light levels when compared to the *Ancylonema* strain from glacier ice (<200 μmol photons m^{-2} s^{-1} vs. 366 μmol photons m^{-2} s^{-1}; Remias & Procházková, 2023). Consistently, a typical low-light (i.e., reduced I_k, increased alpha) or high-light (i.e., increased I_k, reduced alpha) acclimation of the photosystems was noticed. There are, however, significant differences between the photosynthetic performance of the glacier ice alga *A. alaskanum* and the two mesophilic strains, if grown under high light: First, the

light saturation point of the psychrophile was one magnitude higher ($I_k = 472$; Remias & Procházková, 2023) when compared to the mesophiles. Second, the psychrophile reached the highest rETR at very high light levels (rETR of 42 at 1500–2100 μmol photons m^{-2} s^{-1}; Remias & Procházková, 2023). Third, the glacier ice alga showed very low utilization efficiency at low light (alpha = 0.09; Remias & Procházková, 2023). In contrast, the mesophiles showed no chlorophyll fluorescence from 1000 μmol photons m^{-2} s^{-1} but were able to keep a high utilization efficiency at low light levels, irrespective of the acclimation conditions. Overall, these differences indicate that *Ancylonema* strains from the two very different habitat types (moorlands vs. glaciers) display pronounced ecological adaptations.

Interestingly, the mesophilic *Anyclonema* strains produce a secondary pigmentation, which is surprisingly similar to that found in the glacier species. Based on the visual resemblance of the pigmented cells and the phylogenetic proximity of the algae, we assume that the pigmentation is based on the same or similar phenolic compounds as those detected in *A. alaskanum*, namely purpurogallin derivates (Remias, Schwaiger, et al., 2012). Even though the role of these substances as sunscreen is likely, other functions have been proposed as well. For example, antimicrobial effects and an ice-melting function through heat dissipation (Dial et al., 2018; Remias, Schwaiger, et al., 2012). Most of the currently known zygnematophytes that produce striking intracellular pigments (e.g. *Zygogonium ericetorum*, *Temnogametum iztacalense*, psychrophilic *Ancylonema* species) are either uncultivated or difficult to grow, as they occur in extreme habitats in terms of temperature and/or nutrient composition (Aigner et al., 2013; Garduño-Solórzano et al., 2021; Remias et al., 2009). Here, we used our well-growing cultures of *A. palustre* to test for abiotic-inducing factors of intracellular zygnematophycean pigments and found that both nutrient availability and radiation influence secondary pigment biosynthesis. It might seem remarkable that P/N limitation alone lead to a slight reddish pigmentation in *A. palustre* (esp. over longer periods), while this was not regularly observed in richer media (e.g. Waris-H). However, the habitats of *A. palustre* were oligotrophic (strain N3) or dystrophic (strain V5), so a culture medium poor in nitrate and phosphate might better reflect natural nutrient conditions and favour a close-to-natural metabolism – including the production of phenolic pigments. A very strong induction was observed under ultraviolet radiation, in particular UVB, which suggests that the reddish-brown pigments in *Ancylonema* are indeed specific reactions to harmful wavebands. Even though we cannot exclude that the strong vacuolar pigmentation has other functions, especially in psychrophilic strains (e.g., as ice-melting agent to create liquid water and liberate nutrients), the occurrence of these pigments in mesophilic strains and their induction by UVB support an important role in photoprotection.

With these experiments, we optimized the experimental production of the intracellular phenolics of zygnematophytes and were able to create strongly pigmented cells with a close-to-natural phenotype in the laboratory. This paves the way for molecular and analytical follow-up studies on how these pigments are composed and synthesized. In particular, genomic techniques, which often depend on high cell numbers, will be applicable to *A. palustre* and may help to answer the question of how psychrophiles evolved in one particular lineage of zygnematophytes.

TAXONOMY

Class **Zygnematophyceae** Round ex Guiry, 2013.

Genus ***Ancylonema*** Berggren, 1872.

Ancylonema palustre sp. nov.

Description: Cells rod-shaped, 6–8 μm wide and 16–34 μm long, with rounded apices. Two parietal or axial chloroplasts per cell, with smooth edges and a single more or less circular pyrenoid per chloroplast of about 2.5 μm. Nucleus vesicular, about 3.6 μm in diameter, often located in the cell's centre between the chloroplasts, with spherical nucleolus of about 1.7 μm. Cytoplasm is colourless or reddish due to secondary pigments. Zygospores form outside of parent cells, with three cell walls including a multifaceted (dodecahedron-like), colourless mesospore, 13–21 μm in diameter.

Etymology: The species name is derived from *paluster* (neuter *palustre*) [Latin] = living in the swamp; referring to the natural habitat.

Holotype (here designated): Permanent slide with fixed material of strain N3 deposited in *Herbarium Berolinense* (Botanic Garden and Botanical Museum Berlin, B), accession B 40 0045801, locality: Neuenhähnen, North Rhine-Westphalia, Germany; collected 2020, leg. S. Hess.

Type generating strain: N3 (CCAC 9547).

Reference sequence: PP555607 (rbcL gene sequence of strain N3).

PhycoBank ID: http://phycobank.org/104622

AUTHOR CONTRIBUTIONS

Anna Busch: Conceptualization; investigation; writing – original draft; visualization; writing – review and editing; formal analysis. **Emilia Slominski:** Investigation; writing – review and editing; formal analysis. **Daniel Remias:** Investigation; writing – review and editing; resources; formal analysis. **Lenka Procházková:** Visualization; writing – review and editing; formal analysis. **Sebastian Hess:** Conceptualization; funding

acquisition; writing – review and editing; formal analysis; resources.

ACKNOWLEDGEMENTS

This work was funded by the German Research Foundation through the Emmy Noether program, grant 417585753, and the individual research grant 491244984, both to Sebastian Hess. We acknowledge the permission to sample in the Fauna-Flora-Habitat (FFH) Area 'Quellmoor bei Neuenhähnen' granted by the environmental office of the Oberberg district (Germany) and thank Ruth Bruker (University of Cologne) for assistance with scanning electron microscopy. Lenka Procházková was supported by University Research Centers (UNCE) at the Charles University No. UNCE/24/SCI/006 and acknowledges the Czech Science Foundation (GACR), project 24-10019S. Daniel Remias was supported by the Austrian Science Fund (FWF), grant P34073. Open Access funding enabled and organized by Projekt DEAL.

CONFLICT OF INTEREST STATEMENT

The authors declare no conflict of interest.

DATA AVAILABILITY STATEMENT

Sequence data are available in GenBank (https://www.ncbi.nlm.nih.gov/genbank/) under the accessions PP555606, PP555607, PP555608 (*rbc*L gene) and PP544794, PP544795 (18S rRNA gene). Supplementary video files are available in Zenodo: https://zenodo.org/doi/10.5281/zenodo.12708605 (Movie S1: Time-lapse movie of cell division in strain N3; Movie S2: Time-lapse movie of zygospore formation in strain V5).

ORCID

Anna Busch https://orcid.org/0000-0002-5377-7150

REFERENCES

Aigner, S., Remias, D., Karsten, U. & Holzinger, A. (2013) Unusual phenolic compounds contribute to ecophysiological performance in the purple-coloured green alga Z ygogonium ericetorum (Zygnematophyceae, Streptophyta) from a high-alpine habitat. *Journal of Phycology*, 49(4), 648–660.

Barcytė, D., Pilátová, J., Mojzeš, P. & Nedbalová, L. (2020) The arctic Cylindrocystis (Zygnematophyceae, Streptophyta) green algae are genetically and morphologically diverse and exhibit effective accumulation of polyphosphate. *Journal of Phycology*, 56(1) Article 1, 217–232.

Brook, A.J. & Williamson, D.B. (2010) *A monograph on some British desmids*. London, UK: The Ray Society, p. 364.

Busch, A. & Hess, S. (2022a) A diverse group of underappreciated zygnematophytes deserves in-depth exploration. *Applied Phycology*, 3, 1–18.

Busch, A. & Hess, S. (2022b) Sunscreen mucilage: a photoprotective adaptation found in terrestrial green algae (Zygnematophyceae). *European Journal of Phycology*, 57(1), 107–124. Available from: https://doi.org/10.1080/09670262.2021.1898677

Coesel, P.F.M. & Meesters, K.J. (2007) *Desmids of the lowlands: Mesotaeniaceae and Desmidiaceae of the European lowlands*. Amsterdam, The Netherlands: BRILL.

Cook, J.M., Tedstone, A.J., Williamson, C., McCutcheon, J., Hodson, A.J., Dayal, A. et al. (2020) Glacier algae accelerate melt rates on the southwestern Greenland ice sheet. *The Cryosphere*, 14(1), 309–330. Available from: https://doi.org/10.5194/tc-14-309-2020

Dial, R.J., Ganey, G.Q. & Skiles, S.M. (2018) What color should glacier algae be? An ecological role for red carbon in the cryosphere. *FEMS Microbiology Ecology*, 94(3), fiy007. Available from: https://doi.org/10.1093/femsec/fiy007

Fürst-Jansen, J.M.R., de Vries, S. & de Vries, J. (2020) Evo-physio: on stress responses and the earliest land plants. *Journal of Experimental Botany*, 71(11), 3254–3269. Available from: https://doi.org/10.1093/jxb/eraa007

Garduño-Solórzano, G., Martínez-García, M., Scotta Hentschke, G., Lopes, G., Castelo Branco, R., Vasconcelos, V.M.O. et al. (2021) The phylogenetic placement of Temnogametum (Zygnemataceae) and description of Temnogametum iztacalense sp. nov., from a tropical high mountain lake in Mexico. *European Journal of Phycology*, 56(2), 159–173. Available from: https://doi.org/10.1080/09670262.2020.1789226

Geiger, R. (1954) Klassifikation der klimate nach W. Köppen. In: *Landolt-Börnstein: Zahlenwerte und Funktionen aus Physik, Chemie, Astronomie, Geophysik und Technik*, Vol. 3. Berlin, Germany: Springer, pp. 603–607.

Gontcharov, A.A., Marin, B. & Melkonian, M. (2004) Are combined analyses better than single gene phylogenies? A case study using SSU rDNA and rbc L sequence comparisons in the Zygnematophyceae (Streptophyta). *Molecular Biology and Evolution*, 21(3), 612–624.

Hall, J.D. & McCourt, R.M. (2015) Chapter 9—conjugating green algae including desmids. In: Wehr, J.D., Sheath, R.G. & Kociolek, J.P. (Eds.) *Freshwater algae of North America*, 2nd edition. Cambridge, MA: Academic Press, pp. 429–457. Available from: https://doi.org/10.1016/B978-0-12-385876-4.00009-8

Hogetsu, T. & Yokoyama, M. (1979) Light, a nitrogen-depleted medium and cell-cell interaction in the conjugation process of Closterium ehrenbergii Meneghini. *Plant and Cell Physiology*, 20(4), 811–817. Available from: https://doi.org/10.1093/oxfordjournals.pcp.a075873

Jensen, M.B., Perini, L., Halbach, L., Jakobsen, H., Haraguchi, L., Ribeiro, S. et al. (2023) The dark art of cultivating glacier ice algae. *Botany Letters*, 1–10. Available from: https://doi.org/10.1080/23818107.2023.2248235

Kol, E. (1942) *The snow and ice algae of Alaska*, Vol. 101(16). Washington: The Smithsonian Institution, pp. 1–36.

Ling, H.U. & Seppelt, R.D. (1990) Snow algae of the Windmill Islands, continental Antarctica. Mesotaenium berggrenii (Zygnematales, Chlorophyta) the alga of grey snow. *Antarctic Science*, 2(2), 143–148. Available from: https://doi.org/10.1017/S0954102090000189

McFadden, G.I. & Melkonian, M. (1986) Use of HEPES buffer for microalgal culture media and fixation for electron microscopy. *Phycologia*, 25(4), 551–557.

Medlin, L., Elwood, H.J., Stickel, S. & Sogin, M.L. (1988) The characterization of enzymatically amplified eukaryotic 16S-like rRNA-coding regions. *Gene*, 71(2), 491–499. Available from: https://doi.org/10.1016/0378-1119(88)90066-2

Moye, J., Schenk, T. & Hess, S. (2022) Experimental evidence for enzymatic cell wall dissolution in a microbial protoplast feeder (Orciraptor agilis, Viridiraptoridae). *BMC Biology*, 20(1), 267. Available from: https://doi.org/10.1186/s12915-022-01478-x

Permann, C., Herburger, K., Felhofer, M., Gierlinger, N., Lewis, L.A. & Holzinger, A. (2021) Induction of conjugation and Zygospore Cell Wall characteristics in the alpine Spirogyra mirabilis (Zygnematophyceae, Charophyta): advantage under climate change scenarios? *Plants*, 10(8), 1740. Available from: https://doi.org/10.3390/plants10081740

Permann, C., Herburger, K., Niedermeier, M., Felhofer, M., Gierlinger, N. & Holzinger, A. (2021) Cell wall characteristics during sexual reproduction of Mougeotia sp. (Zygnematophyceae) revealed by electron microscopy, glycan microarrays and RAMAN spectroscopy. *Protoplasma*, 258(6), 1261–1275. Available from: https://doi.org/10.1007/s00709-021-01659-5

Permann, C., Gierlinger, N. & Holzinger, A. (2022) Zygospores of the green alga spirogyra: new insights from structural and chemical imaging. *Frontiers in Plant Science*, 13, 1080111. Available from: https://doi.org/10.3389/fpls.2022.1080111

Permann, C., Pichrtová, M., Šoljaková, T., Herburger, K., Jouneau, P.-H., Uwizeye, C. et al. (2023) 3D-reconstructions of zygospores in Zygnema vaginatum (Charophyta) reveal details of cell wall formation, suggesting adaptations to extreme habitats. *Physiologia Plantarum*, 175(4), e13988. Available from: https://doi.org/10.1111/ppl.13988

Pichrtová, M., Holzinger, A., Kulichová, J., Ryšánek, D., Šoljaková, T., Trumhová, K. et al. (2018) Molecular and morphological diversity of Zygnema and Zygnemopsis (Zygnematophyceae, Streptophyta) from Svalbard (high Arctic). *European Journal of Phycology*, 53(4), 492–508.

Poulíčková, A., Žižka, Z., Hašler, P. & Benada, O. (2007) Zygnematalean zygospores: morphological features and use in species identification. *Folia Microbiologica*, 52(2), 135–145. Available from: https://doi.org/10.1007/BF02932152

Procházková, L., Remias, D., Řezanka, T. & Nedbalová, L. (2018) Chloromonas nivalis subsp. tatrae, subsp. nov. (Chlamydomonadales, Chlorophyta): Re–examination of a snow alga from the high Tatra Mountains (Slovakia). *Fottea (Praha)*, 18(1), 1–18. Available from: https://doi.org/10.5507/fot.2017.010

Procházková, L., Řezanka, T., Nedbalová, L. & Remias, D. (2021) Unicellular versus filamentous: the glacial alga Ancylonema alaskana comb. et stat. nov. and its ecophysiological relatedness to Ancylonema nordenskioeldii (Zygnematophyceae, Streptophyta). *Microorganisms*, 9(5), 1103. Available from: https://doi.org/10.3390/microorganisms9051103

Remias, D. & Procházková, L. (2023) The first cultivation of the glacier ice alga Ancylonema alaskanum (Zygnematophyceae, Streptophyta): differences in morphology and photophysiology of field vs laboratory strain cells. *Journal of Glaciology*, 69(276), 1080–1084. Available from: https://doi.org/10.1017/jog.2023.22

Remias, D., Holzinger, A. & Lütz, C. (2009) Physiology, ultrastructure and habitat of the ice alga Mesotaenium berggrenii (Zygnemaphyceae, Chlorophyta) from glaciers in the European Alps. *Phycologia*, 48(4), 302–312. Available from: https://doi.org/10.2216/08-13.1

Remias, D., Holzinger, A., Aigner, S. & Lütz, C. (2012) Ecophysiology and ultrastructure of Ancylonema nordenskiöldii (Zygnematales, Streptophyta), causing brown ice on glaciers in Svalbard (high arctic). *Polar Biology*, 35(6) Article 6, 899–908.

Remias, D., Schwaiger, S., Aigner, S., Leya, T., Stuppner, H. & Lütz, C. (2012) Characterization of an UV-and VIS-absorbing, purpurogallin-derived secondary pigment new to algae and highly abundant in M esotaenium berggrenii (Z ygnematophyceae, Chlorophyta), an extremophyte living on glaciers. *FEMS Microbiology Ecology*, 79(3) Article 3, 638–648.

Remias, D., Procházková, L., Nedbalová, L., Benning, L.G. & Lutz, S. (2023) Novel insights in cryptic diversity of snow and glacier ice algae communities combining 18S rRNA gene and ITS2 amplicon sequencing. *FEMS Microbiology Ecology*, 99(12), fiad134. Available from: https://doi.org/10.1093/femsec/fiad134

Stibal, M., Box, J.E., Cameron, K.A., Langen, P.L., Yallop, M.L., Mottram, R.H. et al. (2017) Algae drive enhanced darkening of bare ice on the Greenland ice sheet. *Geophysical Research Letters*, 44(22), 11463–11471. Available from: https://doi.org/10.1002/2017GL075958

Takano, T., Higuchi, S., Ikegaya, H., Matsuzaki, R., Kawachi, M., Takahashi, F. et al. (2019) Identification of 13 Spirogyra species (Zygnemataceae) by traits of sexual reproduction induced under laboratory culture conditions. *Scientific Reports*, 9(1), 7458.

Takeuchi, N. (2001) The altitudinal distribution of snow algae on an Alaska glacier (Gulkana glacier in the Alaska range). *Hydrological Processes*, 15(18), 3447–3459. Available from: https://doi.org/10.1002/hyp.1040

Takeuchi, N., Uetake, J., Fujita, K., Aizen, V.B. & Nikitin, S.D. (2006) A snow algal community on Akkem glacier in the Russian Altai mountains. *Annals of Glaciology*, 43, 378–384. Available from: https://doi.org/10.3189/172756406781812113

Takeuchi, N., Tanaka, S., Konno, Y., Irvine-Fynn, T.D.L., Rassner, S.M.E. & Edwards, A. (2019) Variations in phototroph communities on the ablating bare-ice surface of glaciers on Brøggerhalvøya, Svalbard. *Frontiers in Earth Science*, 7, 4. Available from: https://doi.org/10.3389/feart.2019.00004

Tamura, K., Stecher, G. & Kumar, S. (2021) MEGA11: molecular evolutionary genetics analysis version 11. *Molecular Biology and Evolution*, 38(7), 3022–3027. Available from: https://doi.org/10.1093/molbev/msab120

Tiflickjian, J.D. & Raybum, W.R. (1986) Nutritional requirements for sexual reproduction in Mesotaenium Kramstai (chlorophyta) 1. *Journal of Phycology*, 22(1), 1–8. Available from: https://doi.org/10.1111/j.1529-8817.1986.tb02508.x

Timme, R.E., Bachvaroff, T.R. & Delwiche, C.F. (2012) Broad phylogenomic sampling and the sister lineage of land plants. *PLoS One*, 7(1), e29696.

de Vries, J., de Vries, S., Slamovits, C.H., Rose, L.E. & Archibald, J.M. (2017) How Embryophytic is the biosynthesis of Phenylpropanoids and their derivatives in Streptophyte algae? *Plant and Cell Physiology*, 58(5), 934–945. Available from: https://doi.org/10.1093/pcp/pcx037

de Vries, J., de Vries, S., Curtis, B.A., Zhou, H., Penny, S., Feussner, K. et al. (2020) Heat stress response in the closest algal relatives of land plants reveals conserved stress signaling circuits. *The Plant Journal*, 103(3), 1025–1048. Available from: https://doi.org/10.1111/tpj.14782

Walsby, A.E. (1997) Modelling the daily integral of photosynthesis by phytoplankton: its dependence on the mean depth of the population. *Hydrobiologia*, 349(1), 65–74. Available from: https://doi.org/10.1023/A:1003045528581

Wickett, N.J., Mirarab, S., Nguyen, N., Warnow, T., Carpenter, E., Matasci, N. et al. (2014) Phylotranscriptomic analysis of the origin and early diversification of land plants. *Proceedings of the National Academy of Sciences of the United States of America*, 111(45), E4859–E4868.

Williamson, C.J., Anesio, A.M., Cook, J., Tedstone, A., Poniecka, E., Holland, A. et al. (2018) Ice algal bloom development on the surface of the Greenland ice sheet. *FEMS Microbiology Ecology*, 94(3), fiy025. Available from: https://doi.org/10.1093/femsec/fiy025

Williamson, C.J., Cameron, K.A., Cook, J.M., Zarsky, J.D., Stibal, M. & Edwards, A. (2019) Glacier algae: a dark past and a darker future. *Frontiers in Microbiology*, 10, 1–8. Available from: https://doi.org/10.3389/fmicb.2019.00524

Williamson, C.J., Cook, J., Tedstone, A., Yallop, M., McCutcheon, J., Poniecka, E. et al. (2020) Algal photophysiology drives darkening and melt of the Greenland ice sheet. *Proceedings of the National Academy of Sciences*, 117(11), 5694–5705. Available from: https://doi.org/10.1073/pnas.1918412117

Wodniok, S., Brinkmann, H., Glöckner, G., Heidel, A.J., Philippe, H., Melkonian, M. et al. (2011) Origin of land plants: do conjugating green algae hold the key? *BMC Evolutionary Biology*, 11(1), 104.

Yallop, M.L., Anesio, A.M., Perkins, R.G., Cook, J., Telling, J., Fagan, D. et al. (2012) Photophysiology and albedo-

changing potential of the ice algal community on the surface of the Greenland ice sheet. *The ISME Journal*, 6(12), 2302–2313. Available from: https://doi.org/10.1038/ismej.2012.107

Yamashita, T. & Sasaki, K. (1979) Conditions for the induction of the mating process and changes in contents of carbohydrates and nitrogen compounds during the mating process of spirogyra. *Journal of the Faculty of Science, Hokkaido University*, 11, 279–287.

Yoshimura, Y., Kohshima, S. & Ohtani, S. (1997) A Community of Snow Algae on a Himalayan glacier: change of algal biomass and community structure with altitude. *Arctic and Alpine Research*, 29(1), 126–137. Available from: https://doi.org/10.1080/00040851.1997.12003222

Zwirn, M., Chen, C., Uher, B. & Schagerl, M. (2013) Induction of sexual reproduction in spirogyra clones—does an universal trigger exist? *Fottea*, 13(1), 77–85. Available from: https://doi.org/10.5507/fot.2013.007

SUPPORTING INFORMATION

Additional supporting information can be found online in the Supporting Information section at the end of this article.

How to cite this article: Busch, A., Slominski, E., Remias, D., Procházková, L. & Hess, S. (2024) A mesophilic relative of common glacier algae, *Ancylonema palustre* sp. nov., provides insights into the induction of vacuolar pigments in zygnematophytes. *Environmental Microbiology*, 26(8), e16680. Available from: https://doi.org/10.1111/1462-2920.16680